# TC-VAE: Uncovering Out-of-Distribution Data Generative Factors

**Cristian Meo** [1] **Anirudh Goyal** [2] **Justin Dauwels** [1]

## Abstract

Uncovering data generative factors is the ultimate goal of disentanglement learning. Although many works proposed disentangling generative models able to uncover the underlying generative factors of a dataset, so far no one was able to uncover OOD generative factors (i.e., factors of variations that are not explicitly shown on the dataset). Moreover, the datasets used to validate these models are synthetically generated using a balanced mixture of some predefined generative factors, implicitly assuming that generative factors are uniformly distributed across the datasets. However, real datasets do not present this property. In this work we analyse the effect of using datasets with unbalanced generative factors, providing qualitative and quantitative results for widely used generative models. Moreover, we propose TC-VAE, a generative model optimized using a lower bound of the joint total correlation between the learned latent representations and the input data. We show that the proposed model is able to uncover OOD generative factors on different datasets and outperforms on average the related baselines in terms of downstream disentanglement metrics.

## 1. Introduction

Unsupervised representation learning aims to identify semantically meaningful representations of data without supervision, while capturing the generative factors of variations that describe the structure of the data (Radford et al., 2016; Locatello et al., 2019). According to (Bengio et al., 2013) disentanglement learning holds the answers for understanding the world from observations, generalizing knowledge across different tasks and domains, learning and generating compositional concepts (Higgins et al., 2016; Kim & Mnih, 2018). The goal of disentanglement learning is to identify a set of independent generative factors $\boldsymbol{z}$ that give rise to the observations $\boldsymbol{x}$ via $p(\boldsymbol{x}|\boldsymbol{z})$. Unsupervised disentangling methods are appealing because they impose constraints to encourage independence among latent variables, while assuming no prior knowledge about the ground truth factors (Do & Tran, 2020). Examples of constraints to encourage independence include forcing the variational posterior $q(\boldsymbol{z}|\boldsymbol{x})$ to be similar to a factorial $p(\boldsymbol{z})$ (Burgess & Kim, 2018) and minimizing the Total Correlation (TC) of the learned latent representation $\boldsymbol{z}$ (Kim & Mnih, 2018; Hwang et al., 2021). Although various approaches (Tomczak & Welling, 2018; Watters et al., 2019; Miao et al., 2022) have been proposed to learn and identify properties of objects, such as shape, color and scale (Burgess & Kim, 2018; Watters et al., 2019), the gap between human-like ability to generalize concepts among different domains and unsupervised representation learning models has not been reduced substantially. Indeed, to the best of our knowledge, there are no models able to uncover generative factors of variation that are not explicitly shown in the dataset. However, understanding that an object can have more generative factors besides the ones shown in the dataset is crucial in order to achieve a human-like degree of understanding. Moreover, most disentangling methods have only been shown to perform well on toy datasets (Matthey et al., 2017; Kumar et al., 2017; Chen et al., 2018; Mathieu et al., 2019; Locatello et al., 2019; Watters et al., 2019; Rotman et al., 2022). These datasets usually present basic objects with simple generative factors, such as object shape, color, and scale. Most importantly, they present a balanced distribution of multiplicative combination of the ground truth factors (e.g. each generative factor variation presents the same number of samples within the dataset). Clearly, it is very unlikely that real datasets present simple and balanced generative factors.

### 1.1. Contributions

The contributions of our work are the following:
**C1**: We develop a convex lower bound of the joint total correlation (TC) between the learned latent representation and the input data. The proposed bound aims to balance the importance of each factor of variation, balancing the effect of imbalances and missing generative factors. The proposed model shows the ability to uncover Out-Of-Distribution (OOD) generative factors, showing interpretable and consistent attributes that were not present within the dataset.

[1]TUDelft, Department of Microelectronics, Delft University of Technology, Delft, The Netherlands [2]DeepMind, London, UK. Correspondence to: Cristian Meo <c.meo@tudelft.nl>.

*Arxiv Preprint*

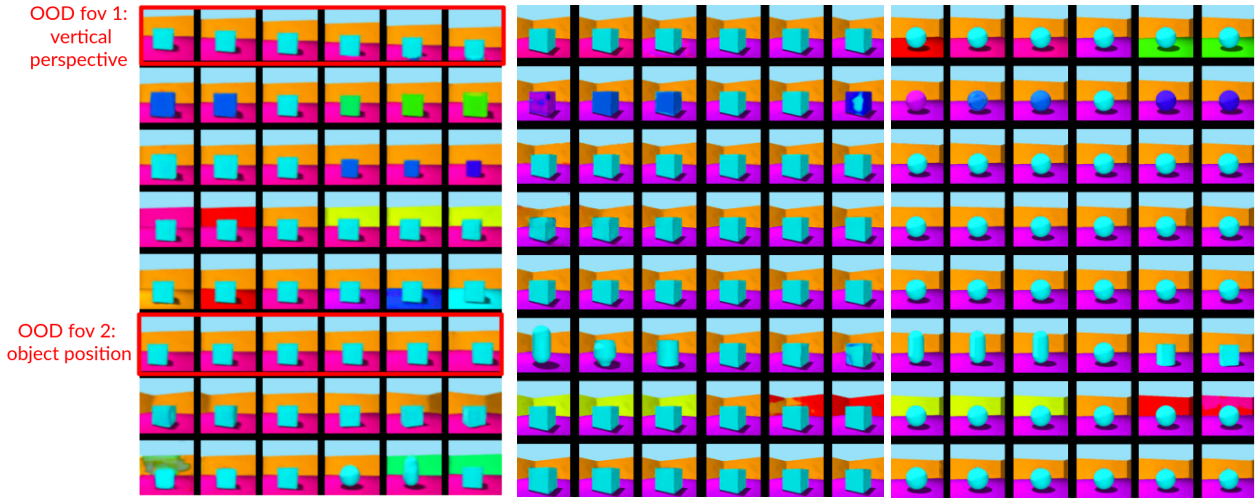


(a) TC-VAE latent traversals (b) FactorVAE latent traversals (c) $\beta$-VAE latent traversals

*Figure 1.* Comparison of generated latent traversals. (a) The generated latent traversals reveals that TC-VAE is able to uncover OOD generative factors of variation (fov) (highlighted in red). However, object dimension and color are not fully disentangled. (b) FactorVAE latent traversals indicates that the learned latent representations are well disentangled. However, some reconstructed images present color inconsistencies. (c) $\beta$-VAE latent traversals are well disentangled. TC-VAE is the only model able to uncover OOD generative factors.

To the best of our knowledge, this is the first model ever proposed that is able to uncover OOD generative factors.

**C2**: We present qualitative and quantitative results that show the effectiveness of the proposed method on a wide range of experiments. Moreover, we introduce a novel strategy to use t-SNE (Van Der Maaten & Hinton, 2008) plots to visualize the learned generative factors of variation in a fully unsupervised way.

**C3**: We conduct quantitative and qualitative analyses of the effect of using dataset with unbalanced combinations of generative factors. Moreover, we propose an unbalanced version of the 3DShapes dataset.

## 2. Related Works

### 2.1. Generative Modeling via Representation Learning

Generative modeling is the task of uncovering the underlying data generative factors and generating novel samples in an unsupervised manner. Variational Autoencoders (VAEs) (Kingma & Welling, 2013; Rezende et al., 2014) are among the most used and widespread classes of generative models. VAEs are explicit-likelihood based generative models, often used to learn a low-dimensional latent representation, that can be used for downstream applications such as image synthesis applications (Razavi et al., 2019; Shi et al., 2020), anomaly detection (Chen et al., 2019), among others. Several VAE-based methods have been presented (Razavi et al., 2019; Peng et al., 2021), showing improvements in generation quality through the use of energy based models (Pandey et al., 2022), diffusion priors (Gu et al., 2022), hierarchical structures (Vahdat & Kautz, 2020), and so on. Meanwhile, another line of work has focused on controllable generative modeling where the aim is to identify directions of variation for each attribute and to manipulate the latent representations of an input image along these directions to generate new images. Examples of controllable generative models are CAGE (Mao et al., 2021), which is able to infer the implicit cause-effect relationships between attributes using causal reasoning (Schölkopf et al., 2021), and DisCo (Härkönen et al., 2020), that uses a contrastive learning approach to discover disentangled directions and learn disentangled representations. As opposed to the mentioned works, our method is able to uncover interpretable generative factors that are not explicitly shown in the dataset. To the best of our knowledge, none of the existing works show this ability.

### 2.2. Disentanglement and Deep Information Bottleneck

It is well known that the difficulty of learning a task, for a given machine learning approach, can vary significantly depending on the choice of data representation. Having a representation that is well suited to the particular task and data domain can significantly improve the learning success rate and robustness of the chosen model (Bengio et al., 2013). Such representations are useful not only for standard downstream tasks such as supervised learning (Alemi et al., 2017) and reinforcement learning (Li, 2017), but also for tasks as transfer learning (Zhuang et al., 2020) and zero-shot learning (Sun et al., 2021). In the last few years, a

link between the latent space capacity and disentanglement of the learned variables (Bengio et al., 2013; Shwartz-Ziv & Tishby, 2017; Goyal et al., 2021) has been identified, showing that decreasing the capacity of a network induces disentanglement on the learned representations. This relationship has been explained by the Information Bottleneck (IB) principle, introduced by (Tishby et al., 2001) as a regularization method to obtain minimal sufficient encoding by constraining the amount of information captured by the latent variables from the observed variable. Deep Variational IB (VIB) (Alemi et al., 2017) has extended the IB framework by applying it to neural networks, which results in a simple yet effective method to learn representations that generalize well and are robust against adversarial attacks. Furthermore, (Alemi et al., 2017; Kirsch et al., 2021) outlined the relationship between VIB, VAE (Kingma & Welling, 2013) and $\beta$-VAE (Higgins et al., 2016), providing an information theoretical interpretation of the Kullback-Leibler (KL) divergence term used in these models as a regularizer. Despite the advantages introduced by the VIB framework, imposing the independence between every latent variable may be too strong an assumption. For this reason, (Fischer & Alemi, 2020) introduced the Conditional Information Bottleneck (CEB), which assumes conditional independence between the learned latent variables, providing the ability to learn more expressive and robust representations (Kirsch et al., 2021). Recently, a generalization of the Mutual Information (MI), namely Total Correlation (TC), has been used to learn disentangled representations as well (Kim & Mnih, 2018; Hwang et al., 2021). Indeed, the TC quantifies the dependency among all dimensions of the single latent variables, making its relationship with the representations disentanglement explicit.

### 2.3. Multi-view Representation Learning

Multi-View Representation Learning (MVRL) aims to learn a combined representation of multiple observations from different types of views or modalities (Hwang et al., 2021). In MVRL, the learned representation must be informative enough to capture the correlation across different modalities without losing view-specific relevant information. The learned representations are then applied to a rich set of downstream tasks. Examples are sensor fusion for multi-sensor systems (Meo et al., 2021; Meo & Lanillos, 2021), clinical diagnosis based on various types of medical records (Zhang et al., 2018), and so on. Several strategies that combine multiple VAEs (i.e., Multimodal VAEs) (Shi et al., 2019; Sutter et al., 2020; 2021) have been proposed to address MVRL, however (Hwang et al., 2021) suggested that these methods have two fundamental limitations: (a) when a subset of views is informative enough to reconstruct the others, the model may rely on those views while ignoring the others, yielding a degenerate solution; (b) while all views are available during training, some of them may not be available at test time. Therefore, these models should be able to infer missing views from the available ones. The same ideas naturally applies to the Unsupervised Representation Learning framework as well: (a) if some factors of variation are informative enough to represent the data structure, the model may learn to rely just on those and ignore the other ones. Moreover, (b) datasets may miss some generative factors among the one used to generate the datasets themselves (i.e., centered-image datasets miss the object position generative factor). To alleviate this problem, (Hwang et al., 2021) proposes MVTCAE, a multimodal VAE optimized using a TC lower bound, showing that the defined TC bound addresses the problem of missing and imbalanced views. Following the same reasoning, we propose a TC lower bound for the unsupervised representation learning case, showing that even in the general framework, the bound helps to alleviate the imbalance and allows the discovery of missing factors (i.e., OOD generative factors).

## 3. TC-VAE Framework Derivation

Let $\mathcal{D} = \{\boldsymbol{X}, \boldsymbol{V}\}$ be the set that consists of images $\boldsymbol{x} \in \mathbb{R}^{N \times N}$, where $N$ indicates the resolution of the image, and a set of conditionally independent ground truth data generative factors $\boldsymbol{v} \in \mathbb{R}^M$, where $\log p(\boldsymbol{v}|\boldsymbol{x}) = \sum_k \log p(v_k|\boldsymbol{x})$. The goal is to develop an unsupervised deep generative model that can learn the joint distribution of the data $\boldsymbol{x}$, while uncovering a set of generative latent factors $\boldsymbol{z}$ ($\boldsymbol{z} \in \mathbb{R}^K$, where $K \geq M$) such that $\boldsymbol{z}$ can fully describe the data structure of $\boldsymbol{x}$ and generate data samples that follow the underlying structure. Since the optimization of the TC is intractable, we are going to maximize a lower bound of the joint Total Correlation $TC(\boldsymbol{z}, \boldsymbol{x})$ between the learned latent representations $\boldsymbol{z}$ and the input data $\boldsymbol{x}$, following the approach proposed by (Hwang et al., 2021). The Total Correlation is defined as the KL divergence between the joint distribution and the factored marginals, and it can be expressed as:

$$TC_\theta(\boldsymbol{z}) \triangleq D_{KL}\left[q_\theta(\boldsymbol{z}) \| \prod_{k=1}^{K} q_\theta(\boldsymbol{z}_k)\right], \tag{1}$$

where the joint distribution is $q_\theta(\boldsymbol{z}) = \int q_\theta(\boldsymbol{z}|\boldsymbol{x}) p_D(\boldsymbol{x}) d\boldsymbol{x}$, $p_D(\boldsymbol{x})$ is the data distribution, $q_\theta(\boldsymbol{z}_k) = \int q_\theta(\boldsymbol{z}|\boldsymbol{x}) d\boldsymbol{z}_{\neq k}$ and $\boldsymbol{z}_{\neq k}$ indicates that the k-th component of $\boldsymbol{z}$ is not considered. Since we aim to find the encoder $q_\theta(\boldsymbol{z}|\boldsymbol{x})$ that disentangles the learned representations $\boldsymbol{z}$, we can formulate the following objective:

$$TC_\theta(\boldsymbol{z}, \boldsymbol{x}) \triangleq TC_\theta(\boldsymbol{z}) - TC_\theta(\boldsymbol{z}|\boldsymbol{x}), \tag{2}$$

where the conditional TC($\boldsymbol{z}|\boldsymbol{x}$) can be expressed as:

$$TC_\theta(\boldsymbol{z}|\boldsymbol{x}) \triangleq \mathbb{E}_{q_\theta(\boldsymbol{z})}\left[D_{KL}\left[q_\theta(\boldsymbol{z}|\boldsymbol{x}) \| \prod_{k=1}^{K} q_\theta(\boldsymbol{z}_k|\boldsymbol{x})\right]\right], \tag{3}$$

which is the expected KL divergence of the joint conditional from the factored conditionals. As for the MVRL

case (Hwang et al., 2021), $TC_\theta(\boldsymbol{z}, \boldsymbol{x})$ is a suitable objective that we can maximise in order to learn complete and disentangled representations $\boldsymbol{z}$. Indeed, Eq. (2) shows that a complete representation should factorize the generative distribution (White et al., 2012; Zhang et al., 2019). Intuitively, we can see that minimizing $TC_\theta(\boldsymbol{z}|\boldsymbol{x})$, $TC_\theta(\boldsymbol{z}, \boldsymbol{x})$ will be maximized, enhancing the completeness and disentanglement of the learned representation $\boldsymbol{z}$. Moreover, decomposing Eq. (2) we can express the TC in terms of MI (Gao et al., 2019):

$$TC_\theta(\boldsymbol{z}, \boldsymbol{x}) = \sum_{k=1}^{K} I_\theta(\boldsymbol{z}_k, \boldsymbol{x}) - I_\theta(\boldsymbol{z}, \boldsymbol{x}), \tag{4}$$

where $I_\theta(\boldsymbol{z}, \boldsymbol{x})$ is the VIB term. Additionally, we can also express it in terms of CMI:

$$TC_\theta(\boldsymbol{z}, \boldsymbol{x}) = \frac{1}{K} \sum_{k=1}^{K} \left[ (K-1) I_\theta(\boldsymbol{z}_k, \boldsymbol{x}) - I_\theta(\boldsymbol{z}_{\neq k}, \boldsymbol{x}|\boldsymbol{z}_k) \right], \tag{5}$$

where $I_\theta(\boldsymbol{z}_{\neq k}, \boldsymbol{x}|\boldsymbol{z}_k)$ is the CEB term. Equations (4) and (5) illustrate the link of the designed objective to both VIB and CEB frameworks. A complete derivation of them can be found in Appendices A.1 and A.2, respectively. While $I_\theta(\boldsymbol{z}_k, \boldsymbol{x})$ encourages the single representations to be more informative, the VIB term promotes compression of the latent representation and the CEB term promotes balance between the information related to each latent representation component. Since we want to promote both disentanglement and information balance of the learned latent representation we propose a lower bound that combines VIB and CEB effects. We define the bound as follow:

$$\begin{aligned} TC(\boldsymbol{z}, \boldsymbol{x}) \geq\ & \mathbb{E}_{q_\theta(\boldsymbol{z}|\boldsymbol{x})} \left[ \log p_\phi(\boldsymbol{x}|\boldsymbol{z}) \right] \\ & \underbrace{- \frac{\alpha}{K - \alpha} \sum_{k=1}^{K} D_{KL}(q_\theta(\boldsymbol{z}_k|\boldsymbol{x}) \| r_p(\boldsymbol{z}_p|\boldsymbol{x}))}_{\text{Conditional VIB}} \\ & - \frac{(1-\alpha)}{(1 - \frac{\alpha}{K})} \underbrace{D_{KL}(q_\theta(\boldsymbol{z}|\boldsymbol{x}) \| r(\boldsymbol{z}))}_{\text{VIB}}, \end{aligned} \tag{6}$$

where $\alpha$ is a hyperparameter that trades off VIB and CEB terms. For simplicity, we define $r_p(\boldsymbol{z}_p|\boldsymbol{x}) = N(\mu_p, \sigma_p \boldsymbol{I})$ and $r(\boldsymbol{z}) = N(\mathbf{0}, \boldsymbol{I})$, respectively, where $\mu_p$ and $\sigma_p$ are:

$$\mu_p \triangleq \frac{\sum_{k=1}^{K} \frac{\boldsymbol{\mu}_k}{\boldsymbol{\sigma}_k^2}}{\sum_{k=1}^{K} \frac{1}{\boldsymbol{\sigma}_k^2}} \quad \text{and} \quad \sigma_p^2 \triangleq \frac{1}{\sum_{k=1}^{K} \frac{1}{\boldsymbol{\sigma}_k^2}} \tag{7}$$

The derived TC lower bound recalls the structure of widely used bounds designed in $\beta$-VAE (Higgins et al., 2016) and FactorVAE (Kim & Mnih, 2018), presenting a marginal log-likelihood term that is responsible of the image reconstruction quality, a VIB term that imposes a bottleneck on the information retained by the latent representation and a CEB term that imposes a structure to the information flowing trough $\boldsymbol{z}$, balancing it across every latent representation variable $\boldsymbol{z}_k$. TC-VAE, $\beta$-VAE and FactorVAE lower bounds are compared in Table 3. A full derivation of the bound defined in Eq. (6) can be found in Appendix A.

## 4. Experiments

In this section, we design empirical experiments to understand the performance of TC-VAE and its potential limitations and the effect of using dataset with unbalanced combinations of generative factors, while exploring the following questions: **Q1** How does TC-VAE performs in terms of downstream metrics (i.e., disentanglement metrics) compared to related baselines? **Q2** How robust are TC-VAE and the related baselines to unbalanced variations of datasets in terms of downstream metrics? **Q3** How informative are the representations learned by TC-VAE compared to the ones learned by related baselines? **Q4** Are TC-VAE and the related baselines able to learn the generative factors of variation of the analyzed datasets? In order to answer the defined questions we are going to validate the models on the following datasets and downstream metrics.

### 4.1. Baseline Methods

We compare TC-VAE with two widely used generative models with related objectives and similar or equal number of parameters to TC-VAE, namely $\beta$-VAE (Higgins et al., 2016) and FactorVAE (Kim & Mnih, 2018). Encoder, Decoder and Discriminator architectures were taken from the Pythae repository (Chadebec et al., 2022). Table 3 illustrates the lower bounds of the compared models. Both $\beta$-VAE and FactorVAE models impose a bottleneck on the information flowing through the latent space, aiming to learn disentangled representations. While $\beta$-VAE does this by introducing a $\beta$ hyperparameter that increases the strength of the information bottleneck, FactorVAE introduces a TC regularizer. Since the TC term is intractable, it is approximated using the density-ratio trick (Nguyen et al., 2010) and optimized using an adversarial strategy which involves the use of a discriminator $D(\boldsymbol{z})$ that outputs an estimation of the probability where $\boldsymbol{z}$ is sampled from $q_\theta(\boldsymbol{z})$ rather than from $\prod_{k=1}^{K} q_\theta(\boldsymbol{z}_k)$. A description hyperparameters used in these experiments can be found in appendix D.

### 4.2. Datasets

**Teapots** (Moreno et al., 2016) contains $200,000$ images of size $64 \times 64$. Each image contains a rendered camera-centered teapot which presents a set of $5$ uniformly distributed generative factors of variations: azimuth and elevation, both sampled between $0$ and $2\pi$, and three RGB color channels, each sampled between $0$ and $1$.

**3DShapes** (Burgess & Kim, 2018) contains $480,000$ images of size $64 \times 64$. Each image contains a rendered

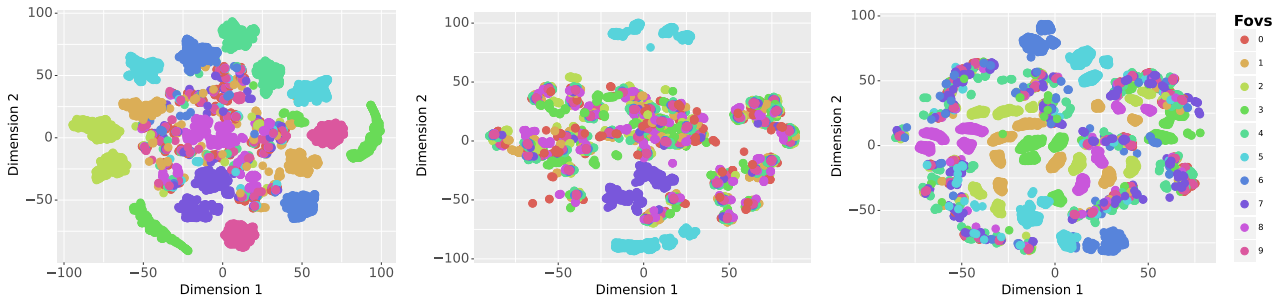


(a) TC-VAE t-SNE (b) FactorVAE t-SNE (c) $\beta$-VAE t-SNE

*Figure 2.* Comparison of t-SNE plots generated using samples obtained by traversing the latent space of TC-VAE, FactorVAE and $\beta$.VAE respectively. The showed labels are the traversals directions, interpreted as generative factors of variation (Fovs). Identifiable clusters represent generative factors of the data. (a) shows that TC-VAE presents 8 different clusters (i.e., 6 i.i.d. generative factors + 2 OOD uncovered ones). (b) FactorVAE contains only two clear clusters. (c) $\beta$-VAE presents 6 clear clusters (i.e. i.i.d. generative factors)

camera-centered object which presents a set of 6 uniformly distributed generative factors of variations: shape sampled from [cylinder, tube, sphere, cube], object color, object hue, floor color, wall color and horizontal orientation, all obtained using linearly spaced values.

**U3DShapes_(100 - P)** Unbalanced 3Dshapes (U3DShapes) is a subset of the 3DShapes dataset, which introduces an unbalance of a generative factor. The $(100 - P)\%$ of the samples contained in the subset depicts cylinders, while the remaining $P\%$ samples contain other objects. All the other generative factors are not modified. As a result, the lower is the percentage P, the higher is the unbalance of the shape generative factor. In the limit of $P = 0$, the object shape is not a generative factor anymore.

**Celeba** (Liu et al., 2015) contains over $200,000$ images of celebrities. Each image depicts a single individual, with a large variety of poses, facial expressions and lighting conditions, and has a resolution of $64 \times 64$ pixels.

Every model is trained using a subset containing the $80\%$ of the selected dataset images in a fully unsupervised way. The models are evaluated on the remaining images using the following downstream scores.

### 4.3. Downstream Scores

**DCI** (Eastwood & Williams, 2018) are used to evaluate the disentanglement and completeness of the learned representations in generative models. $\mathcal{D}$(Disentanglement) measures the degree to which the variation of an individual latent variable $\boldsymbol{z}_k$ corresponds to the variation of a specific generative factor. High $\mathcal{D}$ values indicate that the learned representations are well-disentangled. $\mathcal{C}$(Completeness) measures the average number of variables required to capture a single generative factor. High $\mathcal{C}$ values indicate that each latent variable fully describes a certain factor of variation. DC score, introduced by (Rotman et al., 2022), accounts for both disentanglement and completeness. It is defined as the geometric mean of $\mathcal{D}$ and $\mathcal{C}$, such that only cases where both scores are high will result in a high DC-score. $\mathcal{I}$ (Informativeness) measures how each latent variable $\boldsymbol{z}_k$ is informative with respect to each generative factor. Lower $\mathcal{I}$ values indicate that the learned representations are able to retain most of the information in the data.

**WSEPIN** (Do & Tran, 2020) are used to evaluate the disentanglement and informativeness of the learned representations in generative models. WSEPIN measures whether a representation $\boldsymbol{z}_k$ is both separable from the other representations $\boldsymbol{z}_{\neq k}$ and informative with respect to $\boldsymbol{x}$, taking into account the amount of information retained in $\boldsymbol{z}_k$ that is not present in $\boldsymbol{z}_{\neq k}$. This quantity can be found computing for every latent variable $I(\boldsymbol{x}, \boldsymbol{z}_k|\boldsymbol{z}_{\neq k})$, which is the mutual information between $\boldsymbol{x}$ and $\boldsymbol{z}_k$, given $\boldsymbol{z}_{\neq k}$. Although WSEPIN provides similar information about the learned representations, it is grounded on an information-theoretic framework, which makes it more reliable from a theoretical perspective. Moreover, the inconsistency between different proposed metrics has been pointed out in several works (Do & Tran, 2020; Kirsch et al., 2021), which motivates us to consider metrics from different frameworks to evaluate these downstream scores.

## 5. Results

### 5.1. Main Result: OOD Generative Factors Discovery

To visualize whether the generative factors of a dataset were learned by the model, we show the latent traversals on the 3DShapes dataset in Fig. 1 generated by TC-VAE, $\beta$-VAE, and FactorVAE. Interestingly, the traversals of $\boldsymbol{z}_1$ and $\boldsymbol{z}_6$, highlighted in red, reveal that TC-VAE is able to learn generative factors that were not present in the dataset, namely

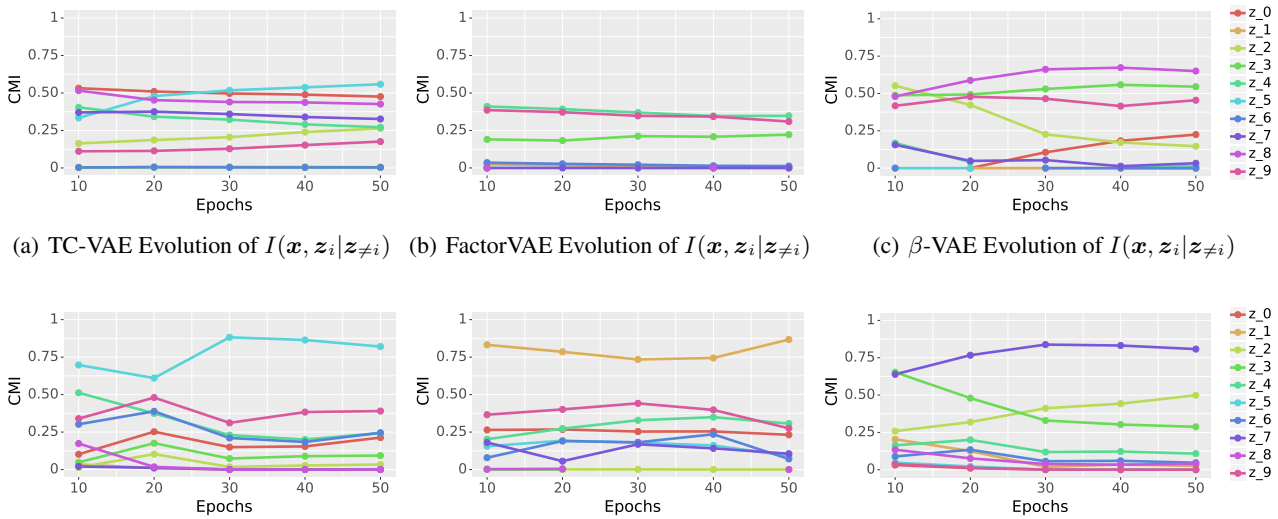


(a) TC-VAE Evolution of $I(\boldsymbol{x}, \boldsymbol{z}_i|\boldsymbol{z}_{\neq i})$ (b) FactorVAE Evolution of $I(\boldsymbol{x}, \boldsymbol{z}_i|\boldsymbol{z}_{\neq i})$ (c) $\beta$-VAE Evolution of $I(\boldsymbol{x}, \boldsymbol{z}_i|\boldsymbol{z}_{\neq i})$

(d) TC-VAE Evolution of $I(\boldsymbol{x}, \boldsymbol{z}_i|\boldsymbol{z}_{\neq i})$ (e) FactorVAE Evolution of $I(\boldsymbol{x}, \boldsymbol{z}_i|\boldsymbol{z}_{\neq i})$ (f) $\beta$-VAE Evolution of $I(\boldsymbol{x}, \boldsymbol{z}_i|\boldsymbol{z}_{\neq i})$

*Figure 3.* Evolution of the Conditional Mutual Information (CMI) $I(\boldsymbol{x}, \boldsymbol{z}_i|\boldsymbol{z}_{\neq i})$ for (a, d) TC-VAE, (b, e) FactorVAE and (c, f) $\beta$-VAE trained on the Teapots (a-c) and 3DShapes (d-f) datasets. TC-VAE latent representations are on average more informative. FactorVAE and $\beta$-VAE present either few or not informative representations. Most of representations informativeness converge already at the 10-th epoch.

vertical perspective, and object position. A comparison of latent traversals on the Teapots and Celeba datasets can be found in Appendices B.2 and B.1, respectively. Figure 7 shows that TC-VAE is able to learn OOD generative factors for the Teapots dataset as well, while in Fig. 6 it presents a rich set of heterogeneous generative factors for Celeba. We argue that the ability of TC-VAE to uncover OOD generative factors comes from the CEB term of its lower bound, showed in Eq. (6), which pushes the latent variables to have a balanced amount of information. Interestingly, all models are able to generate samples showing these OOD attributes (shown in appendix B.3), but TC-VAE is the only one able to give enough importance to these and learn the related generative factors. Instead, FactorVAE and $\beta$-VAE treat these samples as outliers and ignore their generative factors. Moreover, the ability of TC-VAE to uncover OOD factors of variations can be related to the ability of MVT-CAE to infer missing views. According to (Hwang et al., 2021), this ability comes from the CEB term, which balances the information related to each view. Indeed, we can think about OOD generative factors as missing factors. As a result, this term is allowing TC-VAE to learn these OOD generative factors by giving more importance to the samples that present these attributes. However, looking at Fig. 1 (a), we can see that object dimension and color are not fully disentangled. This happens because, since the CEB term balances the amount of information contained by each latent variable, factors of variation that are less informative may be mixed up to reach the average level of informativeness. What is more, Fig. 2 illustrates a comparison of t-SNE (Van Der Maaten & Hinton, 2008) plots created using samples obtained by traversing the latent space. In a nutshell, we explored the latent space by varying each latent variable at a time, as it is commonly done to create the images of latent traversals shown in Fig. 1, we collected the obtained points, and we used them to generate the t-SNE plots, using the traversals directions as labels. Identifiable clusters on these plots represent generative factors of the data. Interestingly, Fig. 2 shows that TC-VAE presents 8 different clusters (i.e., 6 i.i.d. generative factors + 2 OOD uncovered ones). On the other side, $\beta$-VAE t-SNE presents six clear clusters (i.e. i.i.d. generative factors), while the FactorVAE t-SNE plot shows just two clear clusters. Furthermore, the clusters presented in the TC-VAE t-SNE plot seem to be more compact than the baselines ones, which appear fragmented.

### 5.2. Comparison of quantitative results

In order to compare TC-VAE to the related baselines, we evaluated every model on the described datasets. Table 1 illustrates the quantitative results of $\beta$-VAE, FactorVAE, TC-VAE($\alpha = 0.25$), and TC-VAE($\alpha = 0.75$) validated on Teapots, 3DShapes, and Celeba datasets. Each method is evaluated using the presented downstream metrics on three different seeds, and the mean value is reported. A closer look at Table 1 reveals that TC-VAE consistently outperforms the baselines for all datasets in terms of DC score and informativeness (i.e., WSEPIN). Moreover, TC-VAE presents on average better DCI scores, especially in terms of informativeness $\mathcal{I}$ and completeness $\mathcal{C}$, while $\beta$-VAE

*Table 1.* Comparison of downstream performance of $\beta$-VAE, FactorVAE, TC-VAE ($\alpha = 0.25$), and TC-VAE ($\alpha = 0.75$)) validated on three different datasets (Teapots, 3DShapes, and Celeba), using the presented downstream metrics. ($\uparrow$) indicates that higher is better, while for ($\downarrow$) lower is better. The best scores are indicated in **bold**, while the second best ones are underlined. Each experiment was evaluated with three different seeds, and the mean value is reported.

| Dataset | Method | DC | $\mathcal{D}(\uparrow)$ | $\mathcal{C}(\uparrow)$ | $\mathcal{I}(\downarrow)$ | WSEPIN ($\uparrow$) |
|---|---|---|---|---|---|---|
| Teapots | $\beta$-VAE | 0.177 | 0.192 | 0.163 | 0.022 | 0.264 |
| | $\beta$-TCVAE | 0.163 | 0.171 | 0.157 | 0.038 | 0.349 |
| | FactorVAE | 0.384 | 0.456 | 0.324 | 0.017 | 0.215 |
| | TC-VAE($\alpha = 0.25$) | **0.395** | **0.485** | 0.322 | **0.015** | **0.579** |
| | TC-VAE($\alpha = 0.75$) | 0.393 | 0.325 | **0.476** | 0.018 | 0.567 |
| 3DShapes | $\beta$-VAE | 0.288 | **0.383** | 0.216 | 0.037 | 0.406 |
| | $\beta$-TCVAE | 0.310 | 0.374 | 0.258 | 0.038 | 0.349 |
| | FactorVAE | 0.219 | 0.324 | 0.148 | 0.051 | 0.538 |
| | TC-VAE($\alpha = 0.25$) | 0.311 | 0.360 | 0.269 | **0.025** | **0.696** |
| | TC-VAE($\alpha = 0.75$) | **0.312** | 0.291 | **0.334** | 0.040 | 0.556 |
| Celeba | $\beta$-VAE | 0.113 | 0.100 | 0.129 | 0.126 | 0.124 |
| | $\beta$-TCVAE | 0.115 | 0.127 | 0.104 | 0.119 | 0.051 |
| | FactorVAE | 0.103 | 0.093 | 0.113 | 0.142 | 0.111 |
| | TC-VAE($\alpha = 0.25$) | **0.116** | **0.101** | **0.134** | 0.118 | **0.795** |
| | TC-VAE($\alpha = 0.75$) | 0.109 | 0.099 | 0.119 | **0.117** | 0.634 |

outperforms the baselines in terms of disentanglement $\mathcal{D}$ on the 3DShapes dataset. As expected, varying the $\alpha$ hyperparameter has big impact on the downstream performances of TC-VAE. Indeed, the higher is the value of $\alpha$, the lower is the disentanglement $\mathcal{D}$. On average TC-VAE($\alpha = 0.25$) outperforms TC-VAE($\alpha = 0.75$). In agreement with the existing literature (Higgins et al., 2016; Alemi et al., 2017), the VIB term of TC-VAE lower bound is the most important when it comes to downstream performances.

### 5.3. Evolution of Representations Informativeness

To analyze how the informativeness of the learned representations evolves during training, we computed $I(\boldsymbol{x}, \boldsymbol{z}_k|\boldsymbol{z}_{\neq k})$ for every latent variable across the whole training. Fig. 3 shows a comparison of the informativeness evolution for TC-VAE, FactorVAE, and $\beta$-VAE on 3DShapes and Teapots datasets. We can see that TC-VAE latent representations have, on average, higher informativeness. Moreover, while $\beta$-VAE learns fewer latent variables that present high informativeness (i.e., Fig. 3 (c)) , FactorVAE informative representations are fewer and present lower informativeness on the Teapots dataset, as showed from Fig. 3 (b). On the other hand, Fig. 3 (d, e) show that TC-VAE and FactorVAE present similar behaviours on the 3DShapes Dataset. The reason TC-VAE latent representations present a higher degree of informativeness can again be attributed to the effect of the CEB term. Interestingly, most of the informativeness of latent representations converge already at the 10-th epoch on the Teapots dataset, which is reasonable since the samples contain simple objects that are easy to learn.

### 5.4. Comparison of Results on Unbalanced Datasets

To analyse the effect of unbalanced datasets on unsupervised generative models, we present quantitative results of $\beta$-VAE, FactorVAE, TC-VAE($\alpha = 0.25$), and TC-VAE($\alpha = 0.75$) validated on three different unbalanced variations of the 3Dshapes dataset: U3DShapes_75, U3DShapes_50 and U3DShapes_0, where 75, 50 and 0 stand for (100-P). Each method is evaluated using the presented downstream metrics. Table 2 reveals some interesting trends: FactorVAE shows on average better DCI scores, presenting the highest DC score for U3DShapes_50 and U3DShapes_100 datasets. On the other hand, TC-VAE performs the best in terms of informativeness metrics (i.e., $\mathcal{I}$ and WSEPIN). Surprisingly, while WSEPIN maintains comparable order of magnitude with the one found on the i.i.d. case, we observe on average unreasonable stronger DCI scores. Moreover, from Fig. 11, we can see a comparison of the generated latent traversals, which reveals that the generative factors are not well disentangled anymore by none of the models. Therefore, the DCI scores do not show realistic values. Further investigations have to be done to understand why we observe such differences in DCI metrics with respect to the i.i.d. case.

## 6. Discussion

The intuition behind the derivation of the presented TC lower bound comes from the multi-view representation learning framework, where (Hwang et al., 2021) proposes a similar TC bound to alleviate the problem of missing and unbalanced views. Applying the two problems to the unsu-

*Table 2.* Comparison of downstream performance of $\beta$-VAE, FactorVAE, TC-VAE($\alpha = 0.25$), and TC-VAE($\alpha = 0.75$)) validated on three different unbalanced variations of the 3D shapes dataset (U3DShapes_75, U3DShapes_50, U3DShapes_0), using the presented downstream metrics. ($\uparrow$) indicates that higher is better, while for ($\downarrow$) lower is better. The best scores are indicated in **bold**, while the second best ones are underlined. Each experiment was evaluated with three different seeds and the mean value is reported

| Dataset | Method | DC | $\mathcal{D}(\uparrow)$ | $\mathcal{C}(\uparrow)$ | $\mathcal{I}(\downarrow)$ | WSEPIN ($\uparrow$) |
|---|---|---|---|---|---|---|
| U3DShapes_75 | $\beta$-VAE | 0.428 | **0.651** | 0.282 | 0.019 | 0.037 |
| | $\beta$-TCVAE | 0.401 | 0.430 | 0.374 | 0.039 | 0.258 |
| | FactorVAE | 0.524 | 0.527 | 0.521 | 0.030 | 0.429 |
| | TC-VAE($\alpha = 0.25$) | **0.567** | 0.522 | **0.618** | **0.017** | 0.299 |
| | TC-VAE($\alpha = 0.75$) | 0.460 | 0.438 | 0.484 | 0.020 | **0.644** |
| U3DShapes_50 | $\beta$-VAE | 0.469 | 0.509 | 0.433 | 0.022 | 0.312 |
| | $\beta$-TCVAE | 0.416 | 0.420 | 0.413 | 0.024 | 0.242 |
| | FactorVAE | **0.493** | **0.535** | 0.454 | 0.040 | 0.297 |
| | TC-VAE($\alpha = 0.25$) | 0.488 | 0.487 | **0.489** | **0.019** | 0.830 |
| | TC-VAE($\alpha = 0.75$) | 0.422 | 0.397 | 0.449 | 0.021 | **0.949** |
| U3DShapes_0 | $\beta$-VAE | 0.314 | 0.400 | 0.247 | 0.028 | 0.267 |
| | $\beta$-TCVAE | 0.177 | 0.384 | 0.251 | 0.031 | 0.264 |
| | FactorVAE | **0.455** | **0.424** | **0.489** | 0.034 | 0.181 |
| | TC-VAE($\alpha = 0.25$) | 0.356 | 0.394 | 0.321 | **0.025** | **0.607** |
| | TC-VAE($\alpha = 0.75$) | 0.345 | 0.421 | 0.283 | 0.029 | 0.592 |

pervised representation learning framework, we show that these problems are present in this framework as well. Indeed, we can think about missing and unbalanced views as generative factors and realize that the problem of unbalanced views is equivalent to considering data that present unbalanced generative factors. Interestingly, within the literature of disentanglement learning, it has always been assumed that the generative factors are balanced. On the other hand, the problem of inferring missing views can be interpreted as uncovering OOD generative factors that are missing among the ones used to generate the synthetic datasets (i.e., most datasets contain camera-centered objects, the object position generative factor is therefore missing). Considering that the main goal of disentanglement learning is understanding the world from observations (Bengio et al., 2013), we believe that the ability to uncover as many generative factors as possible, OOD ones included, is essential in order to reduce the gap between generative models and human-like ability to understand the world that surrounds us. TC-VAE is the first model able to discover OOD generative factors on two different datasets (e.g., 3DShapes and Teapots) and presents a high heterogeneity on the generative factors uncovered on Celeba. Furthermore, the problem of unbalanced and missing generative factors has a broader impact as well, considering that the representations learned by these models are often used for downstream tasks as well. These problems may lead to the development of models that treat underrepresented generative factors as outliers, neglecting their existence and, therefore, presenting degenerate behaviours. The main limitation of the proposed model is that the CEB term of the derived lower bound decreases the overall disentanglement of the model. Indeed, since it imposes a balance between the information of every latent representation variable, when some generative factors are not very informative, the model tends to mix them up, reducing the overall level of disentanglement. Finally, the experiments conducted on unbalanced versions of the 3DShapes dataset outlined the need for extra investigation on the proposed downstream metrics for disentanglement, especially the DCI metrics (Eastwood & Williams, 2018), which seems to be inconsistent with the generated latent traversals shown on Fig. 11. Indeed, they show that, as soon as the generative factors balance is broken, the generated traversals are not as nicely factorized as they were in the i.i.d. domain.

## 7. Conclusion

Supported by qualitative and quantitative results, we propose TC-VAE, a new generative model that uses a TC lower bound to promote disentanglement while balancing the information retained by every latent representation variable. TC-VAE presents the ability to uncover OOD generative factors, as well as showing on average the best results in terms of disentanglement metrics . Moreover, we highlighted an important gap within the unsupervised representation learning framework: every work ever proposed so far implicitly assumes that the learned generative factors are balanced and fully describe the data, which is a strong assumption for real datasets. We provide both qualitative and quantitative analysis of an unbalanced version of the 3DShapes dataset, which show the limitation of the considered models. In future work, we are going to further investigate the effect of

generative factors unbalance on disentanglement learning and the validity of the related downstream metrics on the unbalanced domain. Moreover, we believe that by applying this model to datasets of real structured objects (i.e., protein structures (Varadi et al., 2021; Irwin et al., 2012)), it may be possible to uncover generative factors that are still unknown and generate new object structures that do not only follow i.i.d. generative factors, besides possibly increasing the understanding of the analyzed objects themselves.

## References


Alemi, A. A., Fischer, I., Dillon, J. V., and Murphy, K. Deep variational information bottleneck. *International Conference on Learning Representations*, 2017.

Bengio, Y., Courville, A., and Vincent, P. Representation learning: A review and new perspectives. *IEEE transactions on pattern analysis and machine intelligence*, 35(8): 1798–1828, 2013.

Burgess, C. and Kim, H. 3d shapes dataset. https://github.com/deepmind/3dshapes-dataset/, 2018.

Chadebec, C., Vincent, L. J., and Allassonnière, S. Pythae: Unifying generative autoencoders in python – a benchmarking use case. *arXiv preprint arXiv:2206.08309*, 2022. URL https://arxiv.org/abs/2206.08309.

Chen, R. T., Li, X., Grosse, R. B., and Duvenaud, D. K. Isolating sources of disentanglement in variational autoencoders. *Advances in neural information processing systems*, 31, 2018.

Chen, W., Xu, H., Li, Z., Pei, D., Chen, J., Qiao, H., Feng, Y., and Wang, Z. Unsupervised anomaly detection for intricate kpis via adversarial training of vae. In *IEEE INFOCOM 2019-IEEE Conference on Computer Communications*, pp. 1891–1899. IEEE, 2019.

Do, K. and Tran, T. Theory and evaluation metrics for learning disentangled representations. In *International Conference on Learning Representations*, 2020. URL https://openreview.net/forum?id=HJgK0h4Ywr.

Eastwood, C. and Williams, C. K. A framework for the quantitative evaluation of disentangled representations. In *International Conference on Learning Representations*, 2018.

Fischer, I. and Alemi, A. A. {CEB} improves model robustness, 2020. URL https://openreview.net/forum?id=SygEukHYvB.

Gao, S., Brekelmans, R., Ver Steeg, G., and Galstyan, A. Auto-encoding total correlation explanation. In *The 22nd International Conference on Artificial Intelligence and Statistics*, pp. 1157–1166. PMLR, 2019.

Goyal, A., Didolkar, A., Ke, N. R., Blundell, C., Beaudoin, P., Heess, N., Mozer, M. C., and Bengio, Y. Neural production systems. *Advances in Neural Information Processing Systems*, 34:25673–25687, 2021.

Gu, S., Chen, D., Bao, J., Wen, F., Zhang, B., Chen, D., Yuan, L., and Guo, B. Vector quantized diffusion model for text-to-image synthesis. In *Proceedings of the IEEE/CVF Conference on Computer Vision and Pattern Recognition*, pp. 10696–10706, 2022.

Härkönen, E., Hertzmann, A., Lehtinen, J., and Paris, S. Ganspace: Discovering interpretable gan controls. *Advances in Neural Information Processing Systems*, 33: 9841–9850, 2020.

Higgins, I., Matthey, L., Pal, A., Burgess, C., Glorot, X., Botvinick, M., Mohamed, S., and Lerchner, A. beta-vae: Learning basic visual concepts with a constrained variational framework. In *International Conference on Learning Representations*, 2016.

Hwang, H., Kim, G.-H., Hong, S., and Kim, K.-E. Multi-view representation learning via total correlation objective. In Ranzato, M., Beygelzimer, A., Dauphin, Y., Liang, P., and Vaughan, J. W. (eds.), *Advances in Neural Information Processing Systems*, volume 34, pp. 12194–12207. Curran Associates, Inc., 2021. URL https://proceedings.neurips.cc/paper/2021/file/65a99bb7a3115fdede20da98b08a370f-Paper.pdf.

Irwin, J. J., Sterling, T., Mysinger, M. M., Bolstad, E. S., and Coleman, R. G. Zinc: A free tool to discover chemistry for biology. *Journal of Chemical Information and Modeling*, 52(7):1757–1768, 2012. doi: 10.1021/ci3001277. URL https://doi.org/10.1021/ci3001277. PMID: 22587354.

Kim, H. and Mnih, A. Disentangling by factorising. In *International Conference on Machine Learning*, pp. 2649–2658. PMLR, 2018.

Kingma, D. P. and Welling, M. Auto-encoding variational bayes. *arXiv preprint arXiv:1312.6114*, 2013.

Kirsch, A., Lyle, C., and Gal, Y. Unpacking information bottlenecks: Surrogate objectives for deep learning, 2021. URL https://openreview.net/forum?id=5rc0K0ezhqI.

Kumar, A., Sattigeri, P., and Balakrishnan, A. Variational inference of disentangled latent concepts from unlabeled observations. *arXiv preprint arXiv:1711.00848*, 2017.

Li, Y. Deep reinforcement learning: An overview. *arXiv preprint arXiv:1701.07274*, 2017.

Liu, Z., Luo, P., Wang, X., and Tang, X. Deep learning face attributes in the wild. In *Proceedings of International Conference on Computer Vision (ICCV)*, December 2015.

Locatello, F., Bauer, S., Lucic, M., Raetsch, G., Gelly, S., Schölkopf, B., and Bachem, O. Challenging common assumptions in the unsupervised learning of disentangled representations. In *international conference on machine learning*, pp. 4114–4124. PMLR, 2019.

Mao, C., Cha, A., Gupta, A., Wang, H., Yang, J., and Vondrick, C. Generative interventions for causal learning. In *Proceedings of the IEEE/CVF Conference on Computer Vision and Pattern Recognition*, pp. 3947–3956, 2021.

Mathieu, E., Rainforth, T., Siddharth, N., and Teh, Y. W. Disentangling disentanglement in variational autoencoders. In *International Conference on Machine Learning*, pp. 4402–4412. PMLR, 2019.

Matthey, L., Higgins, I., Hassabis, D., and Lerchner, A. dsprites: Disentanglement testing sprites dataset, 2017.

Meo, C. and Lanillos, P. Multimodal vae active inference controller. In *2021 IEEE/RSJ International Conference on Intelligent Robots and Systems (IROS)*, pp. 2693–2699. IEEE, 2021.

Meo, C., Franzese, G., Pezzato, C., Spahn, M., and Lanillos, P. Adaptation through prediction: multisensory active inference torque control. *arXiv preprint arXiv:2112.06752*, 2021.

Miao, N., Mathieu, E., N, S., Teh, Y. W., and Rainforth, T. On incorporating inductive biases into VAEs. In *International Conference on Learning Representations*, 2022. URL https://openreview.net/forum?id=nzvbBD_3J-g.

Moreno, P., Williams, C. K., Nash, C., and Kohli, P. Overcoming occlusion with inverse graphics. In *European Conference on Computer Vision*, pp. 170–185. Springer, 2016.

Nguyen, X., Wainwright, M. J., and Jordan, M. I. Estimating divergence functionals and the likelihood ratio by convex risk minimization. *IEEE Transactions on Information Theory*, 56(11):5847–5861, 2010. doi: 10.1109/TIT.2010.2068870.

Pandey, K., Mukherjee, A., Rai, P., and Kumar, A. DiffuseVAE: Efficient, controllable and high-fidelity generation from low-dimensional latents. *Transactions on Machine Learning Research*, 2022. URL https://openreview.net/forum?id=ygoNPRiLxw.

Peng, J., Liu, D., Xu, S., and Li, H. Generating diverse structure for image inpainting with hierarchical vq-vae. In *Proceedings of the IEEE/CVF Conference on Computer Vision and Pattern Recognition*, pp. 10775–10784, 2021.

Radford, A., Metz, L., and Chintala, S. Unsupervised representation learning with deep convolutional generative adversarial networks. *arXiv preprint arXiv:1511.06434*, 2016.

Razavi, A., Van den Oord, A., and Vinyals, O. Generating diverse high-fidelity images with vq-vae-2. *Advances in neural information processing systems*, 32, 2019.

Rezende, D. J., Mohamed, S., and Wierstra, D. Stochastic backpropagation and approximate inference in deep generative models. In *International conference on machine learning*, pp. 1278–1286. PMLR, 2014.

Rotman, M., Dekel, A., Gur, S., Oz, Y., and Wolf, L. Unsupervised disentanglement with tensor product representations on the torus. In *International Conference on Learning Representations*, 2022. URL https://openreview.net/forum?id=neqU3HWDgE.

Schölkopf, B., Locatello, F., Bauer, S., Ke, N. R., Kalchbrenner, N., Goyal, A., and Bengio, Y. Toward causal representation learning. *Proceedings of the IEEE*, 109(5): 612–634, 2021.

Shi, W., Zhou, H., Miao, N., and Li, L. Dispersed exponential family mixture vaes for interpretable text generation. In *International Conference on Machine Learning*, pp. 8840–8851. PMLR, 2020.

Shi, Y., Paige, B., Torr, P., et al. Variational mixture-of-experts autoencoders for multi-modal deep generative models. *Advances in Neural Information Processing Systems*, 32, 2019.

Shwartz-Ziv, R. and Tishby, N. Opening the black box of deep neural networks via information. *arXiv preprint arXiv:1703.00810*, 2017.

Sun, X., Gu, J., and Sun, H. Research progress of zero-shot learning. *Applied Intelligence*, 51(6):3600–3614, 2021.

Sutter, T., Daunhawer, I., and Vogt, J. Multimodal generative learning utilizing jensen-shannon-divergence. *Advances in Neural Information Processing Systems*, 33: 6100–6110, 2020.

Sutter, T. M., Daunhawer, I., and Vogt, J. E. Generalized multimodal elbo. *arXiv preprint arXiv:2105.02470*, 2021.

Tishby, N., Pereira, F. C., and Bialek, W. The information bottleneck method. *Proceedings of the 37th Allerton Conference on Communication, Control and Computation*, 2001.

Tomczak, J. and Welling, M. Vae with a vampprior. In *International Conference on Artificial Intelligence and Statistics*, pp. 1214–1223. PMLR, 2018.

Vahdat, A. and Kautz, J. Nvae: A deep hierarchical variational autoencoder. *Advances in Neural Information Processing Systems*, 33:19667–19679, 2020.

Van Der Maaten, L. and Hinton, G. Visualizing high-dimensional data using t-sne. journal of machine learning research. *J Mach Learn Res*, 9(26):5, 2008.

Varadi, M., Anyango, S., Deshpande, M., Nair, S., Natassia, C., Yordanova, G., Yuan, D., Stroe, O., Wood, G., Laydon, A., Žídek, A., Green, T., Tunyasuvunakool, K., Petersen, S., Jumper, J., Clancy, E., Green, R., Vora, A., Lutfi, M., Figurnov, M., Cowie, A., Hobbs, N., Kohli, P., Kleywegt, G., Birney, E., Hassabis, D., and Velankar, S. AlphaFold Protein Structure Database: massively expanding the structural coverage of protein-sequence space with high-accuracy models. *Nucleic Acids Research*, 50(D1):D439–D444, 11 2021. ISSN 0305-1048. doi: 10.1093/nar/gkab1061. URL https://doi.org/10.1093/nar/gkab1061.

Watters, N., Matthey, L., Burgess, C. P., and Lerchner, A. Spatial broadcast decoder: A simple architecture for learning disentangled representations in vaes. *arXiv preprint arXiv:1901.07017*, 2019.

White, M., Zhang, X., Schuurmans, D., and Yu, Y.-l. Convex multi-view subspace learning. *Advances in neural information processing systems*, 25, 2012.

Zhang, C., Adeli, E., Zhou, T., Chen, X., and Shen, D. Multi-layer multi-view classification for alzheimer's disease diagnosis. In *Proceedings of the AAAI Conference on Artificial Intelligence*, volume 32, 2018.

Zhang, C., Han, Z., Fu, H., Zhou, J. T., Hu, Q., et al. Cpm-nets: Cross partial multi-view networks. *Advances in Neural Information Processing Systems*, 32, 2019.

Zhuang, F., Qi, Z., Duan, K., Xi, D., Zhu, Y., Zhu, H., Xiong, H., and He, Q. A comprehensive survey on transfer learning. *Proceedings of the IEEE*, 109(1):43–76, 2020.

# Appendices

## A. Total Correlation Lower Bound Derivation

In this section we are going to derive the TC lower bound defined in Eq. (6). Since it is defined as a convex combination of marginal log-likelihood, VIB, and CEB terms, we are going to split the derivation into two subsections. First, we will derive a first TC bound that introduces the VIB term. Then, we will derive another TC bound, which explicitly shows the CEB term. Finally, we will define the TC bound shown in Eq. (6) as a convex combination of the two bounds.

### A.1. TC Bound and the Variational Information Bottleneck

Unfortunately, direct optimization of mutual information terms is intractable (Alemi et al., 2017). Therefore, we first need to find a lower bound of Eq. (4). Following the approach used in (Hwang et al., 2021), we can expand it as:

$$
\begin{aligned}
TC_\theta(\boldsymbol{z}, \boldsymbol{x}) &= \sum_{k=1}^{K} I_\theta(\boldsymbol{z}_k, \boldsymbol{x}) - I_\theta(\boldsymbol{z}, \boldsymbol{x}), \\
&= \sum_{k=1}^{K} \left[ \mathbb{E}_{q_\theta(\boldsymbol{x}, \boldsymbol{z}_k)} \left[ \log \frac{q_\theta(\boldsymbol{x}|\boldsymbol{z}_k)}{p_D(\boldsymbol{x})} \right] \right] - \mathbb{E}_{q_\theta(\boldsymbol{x}, \boldsymbol{z})} \left[ \log \frac{q_\theta(\boldsymbol{x}|\boldsymbol{z})}{q_\theta(\boldsymbol{x})} \right], \\
&= \sum_{k=1}^{K} \left[ \mathbb{E}_{q_\theta(\boldsymbol{x}, \boldsymbol{z}_k)} \left[ \log \frac{q_\theta(\boldsymbol{x}|\boldsymbol{z}_k)}{p_D(\boldsymbol{x})} \frac{p_\phi(\boldsymbol{x}|\boldsymbol{z}_k)}{p_\phi(\boldsymbol{x}|\boldsymbol{z}_k)} \right] \right] - \mathbb{E}_{q_\theta(\boldsymbol{z}, \boldsymbol{x})} \left[ \log \frac{q_\theta(\boldsymbol{x}|\boldsymbol{z})}{q_\theta(\boldsymbol{z})} \frac{r(\boldsymbol{z})}{r(\boldsymbol{z})} \right].
\end{aligned} \tag{8}
$$

Let's expand these two terms:

$$
\begin{aligned}
&\mathbb{E}_{q_\theta(\boldsymbol{x}, \boldsymbol{z}_k)} \left[ \log \frac{q_\theta(\boldsymbol{x}|\boldsymbol{z}_k)}{p_D(\boldsymbol{x})} \frac{p_\phi(\boldsymbol{x}|\boldsymbol{z}_k)}{p_\phi(\boldsymbol{x}|\boldsymbol{z}_k)} \right] = \int \int q_\theta(\boldsymbol{z}_k, \boldsymbol{x}) \log \frac{q_\theta(\boldsymbol{x}|\boldsymbol{z}_k)}{p_D(\boldsymbol{x})} \frac{p_\phi(\boldsymbol{x}|\boldsymbol{z}_k)}{p_\phi(\boldsymbol{x}|\boldsymbol{z}_k)} d\boldsymbol{z}_k d\boldsymbol{x}, \\
&= \int \int q_\theta(\boldsymbol{z}_k|\boldsymbol{x}) p_D(\boldsymbol{x}) \left( \log \left( \frac{q_\theta(\boldsymbol{x}|\boldsymbol{z}_k)}{p_\phi(\boldsymbol{x}|\boldsymbol{z}_k)} \right) + \log p_\phi(\boldsymbol{x}|\boldsymbol{z}_k) - \log p_D(\boldsymbol{x}) \right) d\boldsymbol{z}_k d\boldsymbol{x}, \\
&= H(\boldsymbol{x}) + \mathbb{E}_{p_D(\boldsymbol{x})}[D_{KL}(q_\theta(\boldsymbol{x}|\boldsymbol{z}_k) \| p_\phi(\boldsymbol{x}|\boldsymbol{z}_k))] + \mathbb{E}_{q_\theta(\boldsymbol{z}_k|\boldsymbol{x})}[\log p_\phi(\boldsymbol{x}|\boldsymbol{z}_k)].
\end{aligned} \tag{9}
$$

$$
\begin{aligned}
&\mathbb{E}_{q_\theta(\boldsymbol{z}, \boldsymbol{x})} \left[ \log \frac{q_\theta(\boldsymbol{x}|\boldsymbol{z})}{q_\theta(\boldsymbol{z})} \frac{r(\boldsymbol{z})}{r(\boldsymbol{z})} \right], \\
&= \int q_\theta(\boldsymbol{x}, \boldsymbol{z}) \log \left( \frac{q_\theta(\boldsymbol{x}|\boldsymbol{z})}{q_\theta(\boldsymbol{z})} \frac{r(\boldsymbol{z})}{r(\boldsymbol{z})} \right) d\boldsymbol{z} d\boldsymbol{x}, \\
&= \int q_\theta(\boldsymbol{z}|\boldsymbol{x}) p_D(\boldsymbol{x}) \left( \left( \log \frac{q_\theta(\boldsymbol{z}|\boldsymbol{x})}{r(\boldsymbol{z})} \right) + \log \left( \frac{r(\boldsymbol{z})}{q_\theta(\boldsymbol{z})} \right) \right) d\boldsymbol{z} d\boldsymbol{x}, \\
&= \mathbb{E}_{p_D(\boldsymbol{x})}[D_{KL}(q_\theta(\boldsymbol{z}|\boldsymbol{x}) \| r(\boldsymbol{z}))] - \mathbb{E}_{q_\theta(\boldsymbol{x}|\boldsymbol{z})}[[D_{KL}(q_\theta(\boldsymbol{z}) \| r(\boldsymbol{z}))].
\end{aligned} \tag{10}
$$

As a result, we can write:

$$TC_\theta(\boldsymbol{z},\boldsymbol{x}) = \sum_{k=1}^{K}\left[H(\boldsymbol{x}) + \mathbb{E}_{p_D(\boldsymbol{x})}[D_{KL}(q_\theta(\boldsymbol{x}|\boldsymbol{z}_k)\|p_\phi(\boldsymbol{x}|\boldsymbol{z}_k))] + \mathbb{E}_{q_\theta(\boldsymbol{z}_k,\boldsymbol{x})}[\log p_\phi(\boldsymbol{x}|\boldsymbol{z}_k)]\right], \tag{11}$$

$$- \mathbb{E}_{p_D(\boldsymbol{x})}[D_{KL}(q_\theta(\boldsymbol{z}|\boldsymbol{x})\|r(\boldsymbol{z}))] + \mathbb{E}_{q_\theta(\boldsymbol{x}|\boldsymbol{z})}[[D_{KL}(q_\theta(\boldsymbol{z})\|r(\boldsymbol{z}))], \tag{12}$$

$$\begin{aligned}
&\geq \sum_{k=1}^{K}\left[H(\boldsymbol{x}) + \mathbb{E}_{q_\theta(\boldsymbol{z}_k|\boldsymbol{x})}[\log p_\phi(\boldsymbol{x}|\boldsymbol{z}_k)\right] - \mathbb{E}_{p_D(\boldsymbol{x})}[D_{KL}(q_\theta(\boldsymbol{z}|\boldsymbol{x})\|r(\boldsymbol{z}))],\\
&= \sum_{k=1}^{K}\left[H(\boldsymbol{x}) + \int\left(\int q_\theta(\boldsymbol{z}|\boldsymbol{x})d\boldsymbol{z}_{\neq k}\right)\log p_\phi(\boldsymbol{x}|\boldsymbol{z}_k)d\boldsymbol{z}_k d\boldsymbol{x}\right] - \mathbb{E}_{p_D(\boldsymbol{x})}[D_{KL}(q_\theta(\boldsymbol{z}|\boldsymbol{x})\|r(\boldsymbol{z}))],\\
&= \sum_{k=1}^{K}\left[H(\boldsymbol{x}) + \mathbb{E}_{q_\theta(\boldsymbol{z}|\boldsymbol{x})}[\log p_\phi(\boldsymbol{x}|\boldsymbol{z}_k)\right] - \underbrace{\mathbb{E}_{p_D(\boldsymbol{x})}[D_{KL}(q_\theta(\boldsymbol{z}|\boldsymbol{x})\|r(\boldsymbol{z}))]}_{\text{VIB}} =: \mathcal{L}(\boldsymbol{z},\boldsymbol{x}).
\end{aligned} \tag{13}$$

Maximizing $\mathcal{L}(\boldsymbol{z},\boldsymbol{x})$ not only maximizes the original objective $TC(\boldsymbol{z},\boldsymbol{x})$, but at the same time minimize the gap produced by upper bounding Eq. (11). As a result,

$$\sum_{k=1}^{K}\left[\mathbb{E}_{p(\boldsymbol{x})}[D_{KL}(q_\theta(\boldsymbol{x}|\boldsymbol{z}_k)\|p_\phi(\boldsymbol{x}|\boldsymbol{z}_k))]\right] + \mathbb{E}_{q_\theta(\boldsymbol{x}|\boldsymbol{z})}[[D_{KL}(q_\theta(\boldsymbol{z})\|r(\boldsymbol{z}))], \tag{14}$$

will be minimized, leading to: $r(\boldsymbol{z}) \approx q_\theta(\boldsymbol{z})$ and $p_\phi(\boldsymbol{x}|\boldsymbol{z}_k) \approx q_\theta(\boldsymbol{x}|\boldsymbol{z}_k)$.

Moreover, since $H(\boldsymbol{x})$ does not depend on $\theta$, we can drop it from $\mathcal{L}(\boldsymbol{z},\boldsymbol{x})$. Finally, to avoid using a heavy notation, we will denote the VIB term as $D_{KL}(q_\theta(\boldsymbol{z}|\boldsymbol{x})\|r(\boldsymbol{z}))$, leading to the first TC bound which introduces the VIB term:

$$TC_\theta(\boldsymbol{z},\boldsymbol{x}) \geq \mathbb{E}_{q_\theta(\boldsymbol{z}|\boldsymbol{x})}[\log p_\phi(\boldsymbol{x}|\boldsymbol{z})] - \underbrace{D_{KL}(q_\theta(\boldsymbol{z}|\boldsymbol{x})\|r(\boldsymbol{z}))}_{\text{VIB}}. \tag{15}$$

### A.2. TC bound and the Conditional Variational Information Bottleneck

Expanding Eq. (2), we can reformulate $TC(\boldsymbol{z},\boldsymbol{x})$ as follow:

$$TC_\phi(\boldsymbol{z},\boldsymbol{x}) = \sum_{k=1}^{K} I_\phi(\boldsymbol{z}_k,\boldsymbol{x}) - I_\phi(\boldsymbol{z},\boldsymbol{x}), \tag{16}$$

$$\begin{aligned}
&= \sum_{k=1}^{K}\left[\frac{K-1}{K}I_\phi(\boldsymbol{z}_k,\boldsymbol{x}) + \frac{1}{K}I_\phi(\boldsymbol{z}_k,\boldsymbol{x}) - \frac{1}{K}I_\phi(\boldsymbol{z},\boldsymbol{x})\right],\\
&= \sum_{k=1}^{K}\left[\frac{K-1}{K}I_\phi(\boldsymbol{z}_k,\boldsymbol{x}) + \frac{1}{K}\left(I_\phi(\boldsymbol{z}_k,\boldsymbol{x}) - I_\phi(\boldsymbol{z},\boldsymbol{x})\right)\right].
\end{aligned} \tag{17}$$

Interestingly, can write the last term of Eq. (17) as:

$$
\begin{aligned}
I_\phi(\boldsymbol{z}_k, \boldsymbol{x}) - I_\phi(\boldsymbol{z}, \boldsymbol{x}) &= \sum_{k=1}^{K} \left[ \mathbb{E}_{p_\phi(\boldsymbol{z}_k, \boldsymbol{x})} \left[ \log \frac{p_\phi(\boldsymbol{x}|\boldsymbol{z}_k)}{p_D(\boldsymbol{x})} \right] \right] - \mathbb{E}_{p_\phi(\boldsymbol{x}, \boldsymbol{z})} \left[ \log \frac{p_\phi(\boldsymbol{x}|\boldsymbol{z})}{p_D(\boldsymbol{x})} \right], \\
&= \int \left( \int p_\phi(\boldsymbol{x}|\boldsymbol{z}) p(\boldsymbol{z}) d\boldsymbol{z}_{\neq \boldsymbol{z}_k} \right) \log \frac{p_\phi(\boldsymbol{x}|\boldsymbol{z}_k)}{p_D(\boldsymbol{x})} d\boldsymbol{z}_k d\boldsymbol{x}, \\
&- \int p_\phi(\boldsymbol{x}|\boldsymbol{z}) p(\boldsymbol{z}) \log \frac{p_\phi(\boldsymbol{x}|\boldsymbol{z}_k)}{p_D(\boldsymbol{x})} d\boldsymbol{z} d\boldsymbol{x}, \\
&= \int p_\phi(\boldsymbol{x}|\boldsymbol{z}) p(\boldsymbol{z}) \log \frac{p_\phi(\boldsymbol{x}|\boldsymbol{z}_k)}{p(\boldsymbol{x}|\boldsymbol{z})} d\boldsymbol{z} d\boldsymbol{x}, \\
&= - \int p_\phi(\boldsymbol{x}|\boldsymbol{z}) p(\boldsymbol{z}) \log \frac{p(\boldsymbol{x}|\boldsymbol{z})}{p_\phi(\boldsymbol{x}|\boldsymbol{z}_k)} d\boldsymbol{z} d\boldsymbol{x}, \\
&= - \int p_\phi(\boldsymbol{x}|\boldsymbol{z}) p(\boldsymbol{z}) \log \frac{p(\boldsymbol{x}|\boldsymbol{z}_{\neq k}, \boldsymbol{z}_k)}{p_\phi(\boldsymbol{x}|\boldsymbol{z}_k)} d\boldsymbol{z} d\boldsymbol{x}, \\
&= -I_\phi(\boldsymbol{z}_{\neq k}, \boldsymbol{x}|\boldsymbol{z}_k).
\end{aligned} \tag{18}
$$

We can now write Eq. (5):

$$
TC_\theta(\boldsymbol{z}, \boldsymbol{x}) = \frac{1}{K} \sum_{k=1}^{K} \left[ (K-1) I_\theta(\boldsymbol{z}_k, \boldsymbol{x}) - I_\theta(\boldsymbol{z}_{\neq k}, \boldsymbol{x}|\boldsymbol{z}_k) \right].
$$

Interestingly, the second IB term in Eq. (8) can now be expressed as multiple conditional MIs between the observation and $K-1$ other latent variables given the k-th latent representation variable, penalizing the extra information of the observation not inferable from the given latent representation variable. Moreover, we can further expand the TC as:

$$
\begin{aligned}
TC_\phi(\boldsymbol{z}, \boldsymbol{x}) &= \sum_{k=1}^{K} \left[ \frac{K-1}{K} I_\phi(\boldsymbol{z}_k, \boldsymbol{x}) + \frac{1}{K} I_\phi(\boldsymbol{z}_k, \boldsymbol{x}) - \frac{1}{K} I_\phi(\boldsymbol{z}, \boldsymbol{x}) \right], \qquad (19) \\
&= \frac{1}{K} \sum_{k=1}^{K} (K-1) \left[ \mathbb{E}_{q_\theta(\boldsymbol{z}_k|\boldsymbol{x})} \left[ \log \frac{p_\phi(\boldsymbol{x}|\boldsymbol{z}_k)}{p_\phi(\boldsymbol{x})} \frac{p(\boldsymbol{x}|\boldsymbol{z}_k)}{p(\boldsymbol{x}|\boldsymbol{z}_k)} \right] \right] - \mathbb{E}_{q_\theta(\boldsymbol{x}, \boldsymbol{z})} \left[ \log \frac{q_\theta(\boldsymbol{z}|\boldsymbol{x})}{q_\theta(\boldsymbol{z}_k|\boldsymbol{x})} \frac{r_p(\boldsymbol{z}|\boldsymbol{x})}{r_p(\boldsymbol{z}|\boldsymbol{x})} \right], \\
&= \frac{K-1}{K} \sum_{k=1}^{K} \left[ H(\boldsymbol{x}) + \mathbb{E}_{q_\theta(\boldsymbol{z}_k, \boldsymbol{x})} [\log p_\phi(\boldsymbol{x}|\boldsymbol{z}_k)] \right] - \frac{1}{K} \sum_{k=1}^{K} \left[ \mathbb{E}_{q_\theta(\boldsymbol{z})} [D_{KL}(q_\theta(\boldsymbol{z}_k|\boldsymbol{x}) \| r_p(\boldsymbol{z}|\boldsymbol{x}))] \right] \\
&+ \frac{K-1}{K} \sum_{k=1}^{K} \left[ \mathbb{E}_{q_\theta(\boldsymbol{z}_k)} [D_{KL}(p_\phi(\boldsymbol{x}|\boldsymbol{z}_k) \| p(\boldsymbol{x}|\boldsymbol{z}_k))] \right] + \frac{1}{K} \sum_{k=1}^{K} \mathbb{E}_{q_\theta(\boldsymbol{z}_{\neq k}|\boldsymbol{x}) p(\boldsymbol{x})} [D_{KL}(q_\theta(\boldsymbol{z}|\boldsymbol{x}) \| r_p(\boldsymbol{z}|\boldsymbol{x})], \qquad (20) \\
&\geq \frac{K-1}{K} \sum_{k=1}^{K} \left[ H(\boldsymbol{x}) + \mathbb{E}_{q_\theta(\boldsymbol{z}_k|\boldsymbol{x})} [\log p_\phi(\boldsymbol{x}|\boldsymbol{z}_k)] \right] - \frac{1}{K} \sum_{k=1}^{K} \left[ \mathbb{E}_{p(\boldsymbol{z})} [D_{KL}(q_\theta(\boldsymbol{z}_k|\boldsymbol{x}) \| r_p(\boldsymbol{z}|\boldsymbol{x})] \right]. \qquad (21)
\end{aligned}
$$

Maximizing Eq. (21) not only maximizes the original objective $TC(\boldsymbol{z}, \boldsymbol{x})$ but at the same time minimizes the gap produced by upper bounding Eq. (20), leading to: $r_p(\boldsymbol{z}|\boldsymbol{x}) \approx q_\theta(\boldsymbol{z}_k|\boldsymbol{x})$, $p_\phi(\boldsymbol{x}|\boldsymbol{z}_k) \approx p_\phi(\boldsymbol{x}|\boldsymbol{z}_k)$.

Moreover, since $H(\boldsymbol{x})$ does not depend on $\theta$, we can drop it from Eq. (21). Finally, to avoid using a heavy notation, we will denote the CEB term as $D_{KL}(q_\theta(\boldsymbol{z}_k|\boldsymbol{x}) \| r_p(\boldsymbol{z}|\boldsymbol{x}))$, leading to the second TC bound which introduces the CEB term:

$$
TC_\theta(\boldsymbol{z}, \boldsymbol{x}) \geq \frac{K-1}{K} \mathbb{E}_{q_\theta(\boldsymbol{z}|\boldsymbol{x})} [\log p_\phi(\boldsymbol{x}|\boldsymbol{z})] - \underbrace{\frac{1}{K} \sum_{k=1}^{K} D_{KL}(q_\theta(\boldsymbol{z}_k|\boldsymbol{x}) \| r_p(\boldsymbol{z}|\boldsymbol{x}))}_{\text{CEB}}. \tag{22}
$$

*Table 3.* This table compares the lower bound objective functions of TC-VAE, $\beta$-VAE, and FactorVAE. The lower bound objective function of $\beta$-VAE is composed of the expected log-likelihood of the data given the latent variables and the KL divergence between the approximate posterior and the prior of the latent variables (i.e., VIB term). The FactorVAE model further adds a KL divergence term between the approximate posterior and the factorized prior of the latent variables, which approximates the total correlation of the latent variables. TC-VAE, on the other hand, uses a convex combination of VIB term and KL divergence between the approximate posterior and the prior of the latent variables conditioned on the k-th latent variable (i.e., CEB term). $K$ represents the dimensionality of the latent variables, while $\beta$, $\gamma$ and $\alpha$ are hyperparameters of the models.

| Model | Lower Bound |
|---|---|
| $\beta$-VAE | $\mathbb{E}_{q_\theta(\boldsymbol{z}\|\boldsymbol{x})}[\log p_\phi(\boldsymbol{x}\|\boldsymbol{z})] - \beta D_{KL}(q_\theta(\boldsymbol{z}\|\boldsymbol{x})\|p(\boldsymbol{z}))$ |
| FactorVAE | $\mathbb{E}_{q_\theta(\boldsymbol{z}\|\boldsymbol{x})}[\log p_\phi(\boldsymbol{x}\|\boldsymbol{z})] - \beta D_{KL}(q_\theta(\boldsymbol{z}\|\boldsymbol{x})\|p(\boldsymbol{z})) - \gamma D_{KL}(q_\theta(\boldsymbol{z})\|\prod_{k=1}^{K} q_\phi(\boldsymbol{z}_k))$ |
| TC-VAE | $\mathbb{E}_{q_\theta(\boldsymbol{z}\|\boldsymbol{x})}\left[\log p_\phi(\boldsymbol{x}\|\boldsymbol{z})\right] - \frac{\alpha}{K-\alpha}\sum_{k=1}^{K} D_{KL}(q_\theta(\boldsymbol{z}\|\boldsymbol{x})\|r_p(\boldsymbol{z}_p\|\boldsymbol{x})) - \frac{(1-\alpha)}{(1-\frac{\alpha}{K})} D_{KL}(q_\theta(\boldsymbol{z}\|\boldsymbol{x})\|r(\boldsymbol{z}))$ |

### A.3. Final TC bound

In order to obtain the final expression of the derived TC bound, we can compute a convex combination of the two bounds defined in Eq. (15) and (22).

$$
\begin{aligned}
TC(\boldsymbol{z},\boldsymbol{x}) &= (1-\alpha)\left(\sum_{k=1}^{K} I_\theta(\boldsymbol{z}_k,\boldsymbol{x}) - I_\theta(\boldsymbol{z},\boldsymbol{x})\right) + \alpha\left(\sum_{k=1}^{K}\left[\frac{K-1}{K} I_\theta(\boldsymbol{z}_k,\boldsymbol{x}) + \frac{1}{K} I_\theta(\boldsymbol{z}_k,\boldsymbol{x}) - \frac{1}{K} I_\theta(\boldsymbol{z},\boldsymbol{x})\right]\right), \quad (23)\\
&= \frac{K(1-\alpha)+\alpha(K-1)}{K}\sum_{k=1}^{K} I_\theta(\boldsymbol{z}_k,\boldsymbol{x}) - \frac{\alpha}{K}\sum_{k=1}^{K}\left(\frac{1}{K} I_\theta(\boldsymbol{z}_k,\boldsymbol{x}) - \frac{1}{K} I_\theta(\boldsymbol{z},\boldsymbol{x})\right) - (1-\alpha) I_\theta(\boldsymbol{z},\boldsymbol{x}),\\
&\geq \frac{K-\alpha}{K}\mathbb{E}_{q_\theta(\boldsymbol{z}|\boldsymbol{x})}\left[\log p_\phi(\boldsymbol{x}|\boldsymbol{z})\right] - \frac{\alpha}{K}\sum_{k=1}^{K} D_{KL}(q_\theta(\boldsymbol{z}_k|\boldsymbol{x})\|r_p(\boldsymbol{z}|\boldsymbol{x})) - (1-\alpha) D_{KL}(p_\theta(\boldsymbol{z}|\boldsymbol{x})\|r(\boldsymbol{z})),\\
&= \mathbb{E}_{q_\theta(\boldsymbol{z}|\boldsymbol{x})}\left[\log p_\phi(\boldsymbol{x}|\boldsymbol{z})\right] - \frac{\alpha}{K-\alpha}\sum_{k=1}^{K} D_{KL}(q_\theta(\boldsymbol{z}_k|\boldsymbol{x})\|r_p(\boldsymbol{z}|\boldsymbol{x})) - \frac{(1-\alpha)}{(1-\frac{\alpha}{K})} D_{KL}(q_\theta(\boldsymbol{z}|\boldsymbol{x})\|r(\boldsymbol{z})).
\end{aligned}
$$

where $\alpha$ is a hyperparameter that balances the effects of VIB and CEB terms. Table 3 illustrates the lower bounds defined for $\beta$-VAE (Higgins et al., 2016) and FactorVAE (Kim & Mnih, 2018), comparing them to the derived TC bound. We can see that the three bounds present a similar structure, presenting a marginal log-likelihood term and either one or two KL regularizers that impose some kind of information bottleneck.

## B. Additional Results

In this section we present some additional results, namely traversals generated for Teapots, Celeba and U3DShapes datasets and generated samples of the 3DShapes dataset.

### B.1. Celeba latent traversals

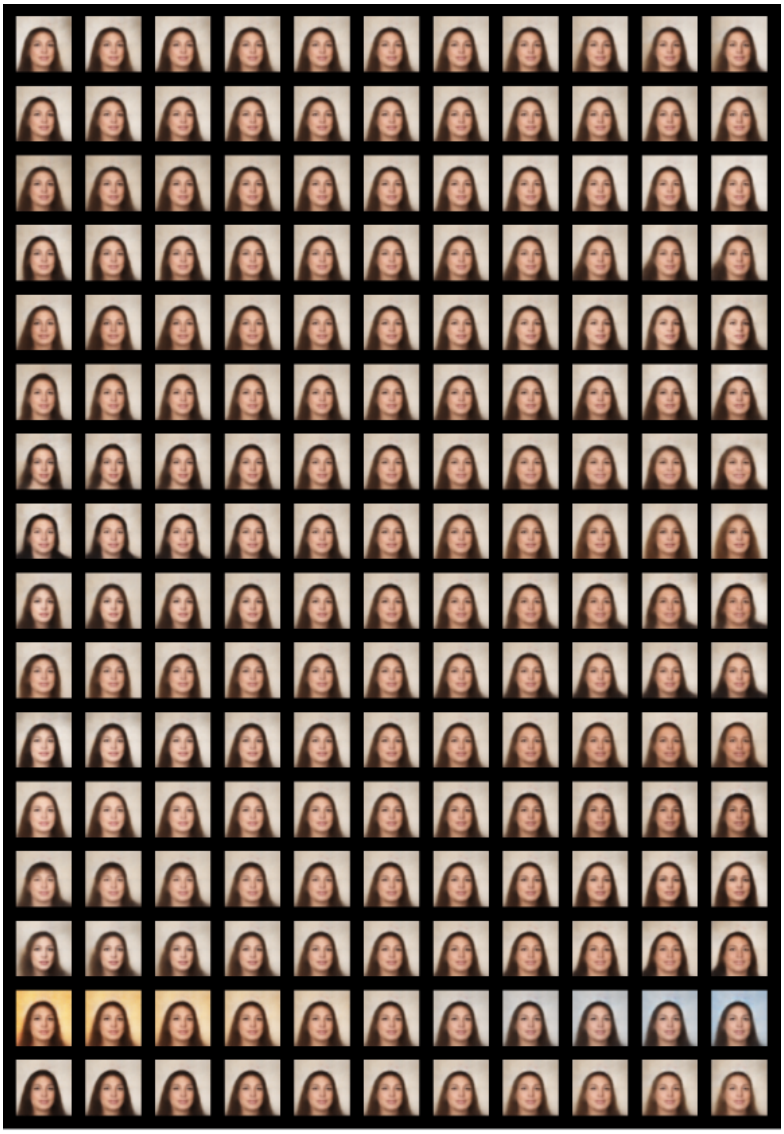

*Figure 4.* $\beta$-VAE traversals of the Celeba Dataset.

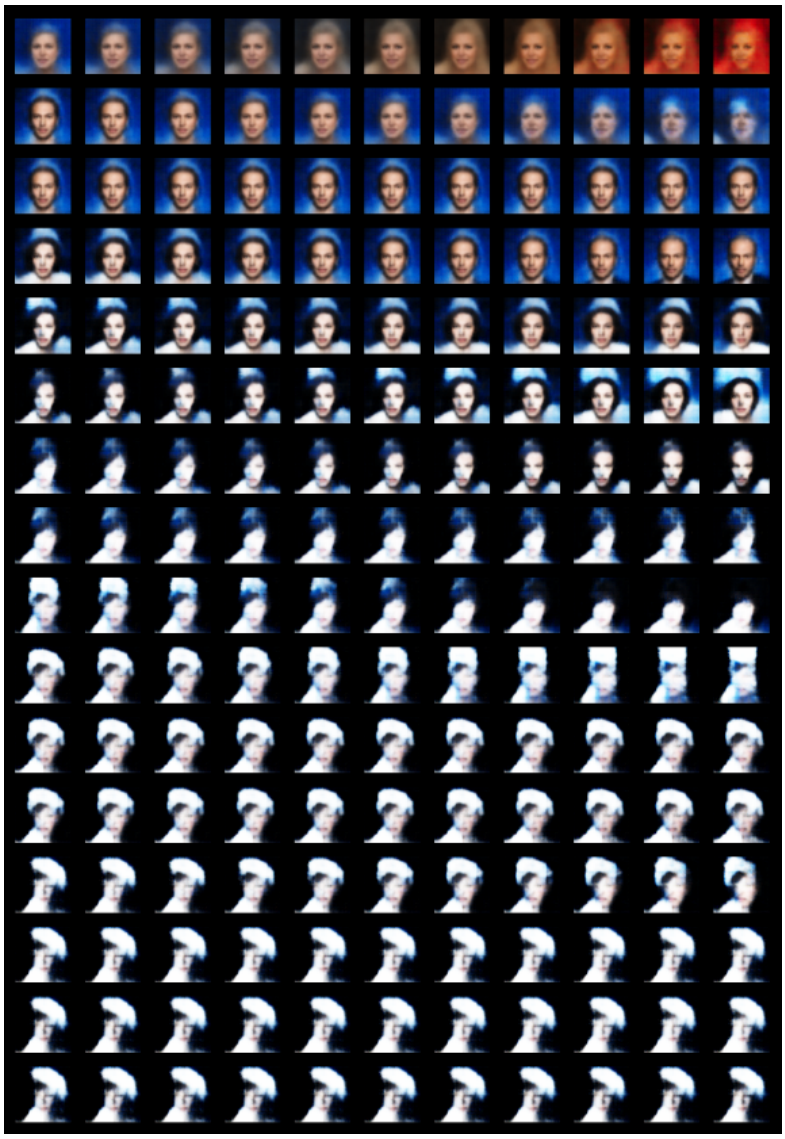

*Figure 5.* FactorVAE traversals of the Celeba Dataset.

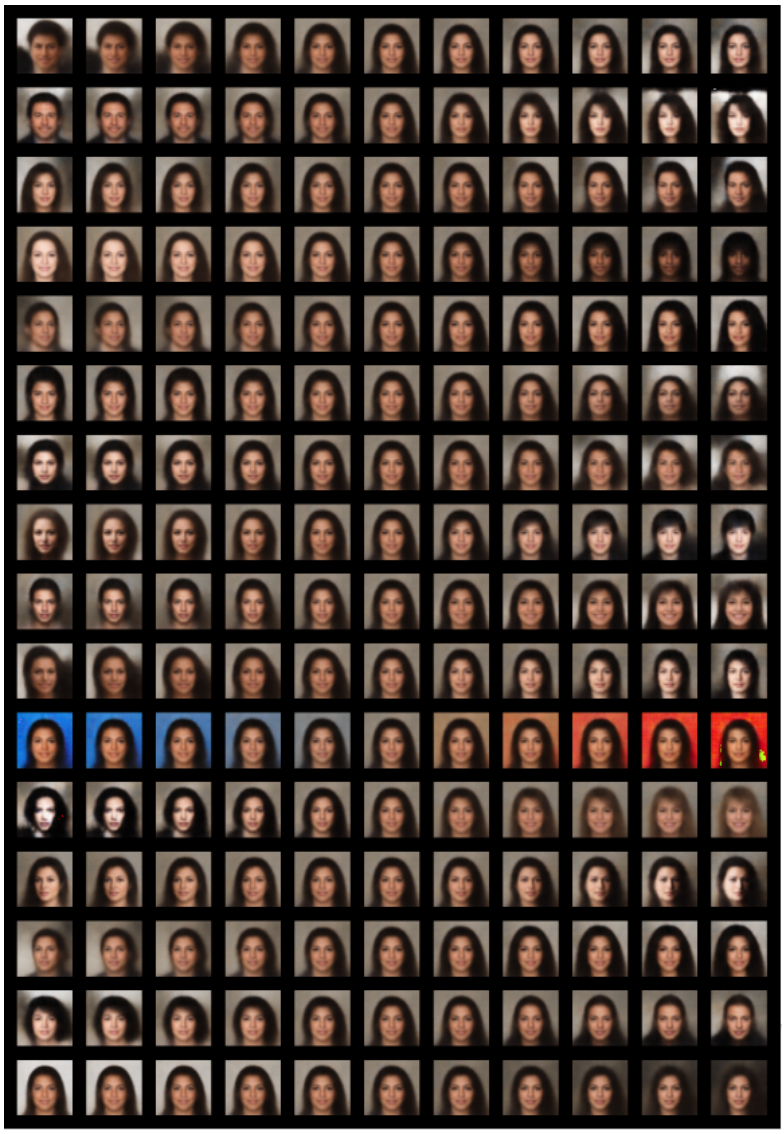

*Figure 6.* TC-VAE traversals of the Celeba Dataset. Each traversal direction seems to contain a different generative factor, presenting a high heterogeneity among the learned factors.

### B.2. Teapots Traversals

(a) TC-VAE latent traversals (b) FactorVAE latent traversals (c) $\beta$-VAE latent traversals

*Figure 7.* Comparison of generated latent traversals. (a) The generated latent traversals reveal that TC-VAE is able to uncover OOD generative factors of variation (i.e., pot position) . (b) FactorVAE latent traversals indicate that the learned latent representations are not well disentangled. (c) $\beta$-VAE latent traversals do not show significant variation in the representations. Additionally, some generative factors are not uncovered.

### B.3. Generated OOD Samples

In this section we present three sets of samples generated by TC-VAE, $\beta$-VAE and FactorVAE, which shows OOD attributes. Interestingly, although TC-VAE is only one able to uncover the OOD generative factors related to these attributes, all models are able to generate samples containing these attributes (i.e., vertical perspective, object position). However, Fig. 8 clearly shows that OOD samples generated by TC-VAE presents a much better reconstruction quality.

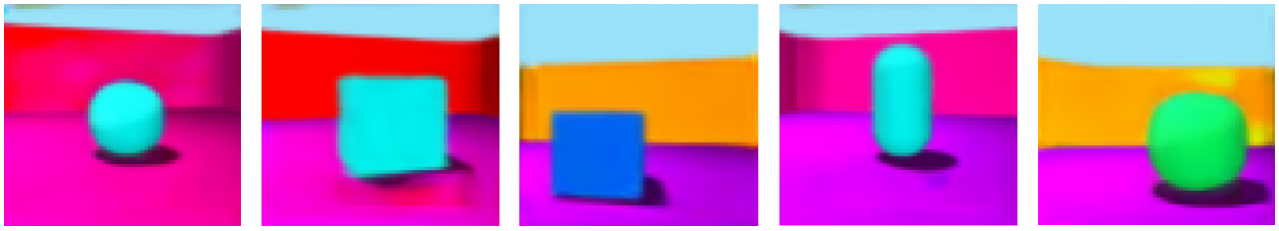

*Figure 8.* OOD samples generated by TC-VAE.

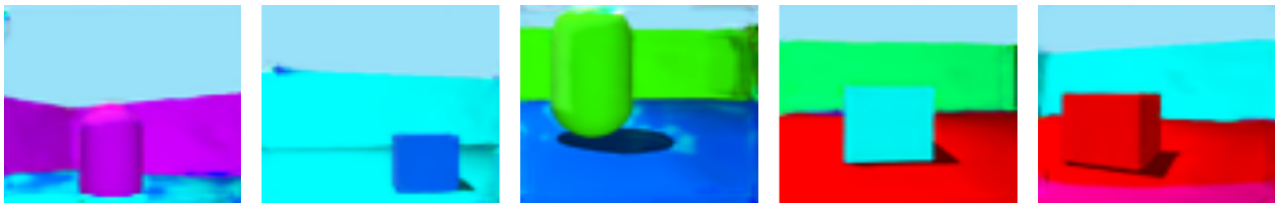

*Figure 9.* OOD samples generated by $\beta$-VAE.

*Figure 10.* OOD samples generated by FactorVAE.

## C. Unbalanced 3DShapes Traversals

In this section we present latent traversals generated by TC-VAE, FactorVAE and $\beta$-VAE validate on an unbalanced version of the 3DShapes dataset, namely U3DShapes_75. Although we can see that the other objects shape are learned, the disentanglement showed on the traversals generated within the i.i.d. domain (Fig. 1) is lost. This evidence highlights the need of further investigation of the effect of unbalanced generative factors in disentanglement learning.

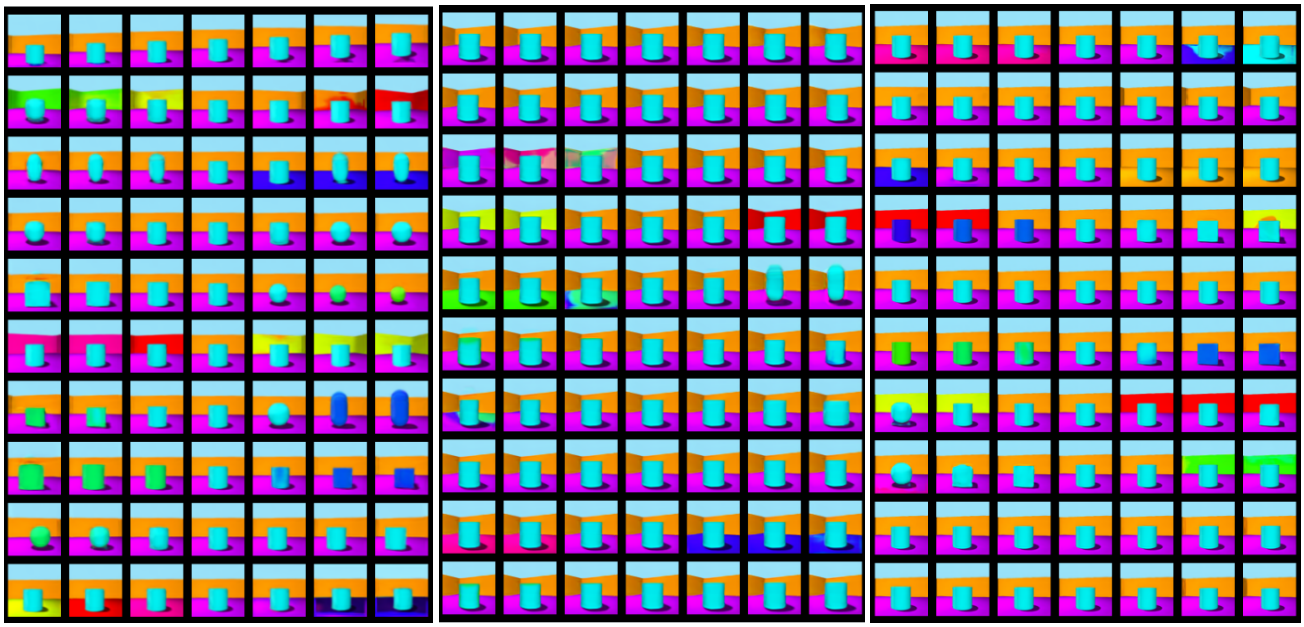

(a) TC-VAE latent traversals (b) FactorVAE latent traversals (c) $\beta$-VAE latent traversals

*Figure 11.* Comparison of generated latent traversals of (a) TC-VAE, (b) FactorVAE and (c) $\beta$-VAE, validated on the U3Dshapes_75 dataset.

## D. Architectures and Hyperparameters Details

The hyperparameters used for the different experiments are showed on Table 4.

*Table 4.* Comparison of the different hyperparameters used across the Datasets

| Dataset | $\beta$ | $\gamma$ | $\alpha$ | latent dim K | Training Epochs |
|---|---|---|---|---|---|
| Teapots | 2 | 10 | (0.25, 0.75) | 10 | 50 |
| 3DShapes | 3 | 10 | (0.25, 0.75) | 10 | 50 |
| U3DShapes | 3 | 10 | (0.25, 0.75) | 10 | 50 |
| Celeba | 5 | 10 | (0.25, 0.75) | 16 | 100 |

The Encoder, Decoder and Discriminator architecture are taken from the Pythae package (Chadebec et al., 2022).